

Performance of Conformal Prediction in Capturing Aleatoric Uncertainty

Misgina Tsighe Hagos¹ Claes Lundström^{1,2}

¹Linköping University ²Sectra AB

Abstract

Conformal prediction is a model-agnostic approach to generating prediction sets that cover the true class with a high probability. Although its prediction set size is expected to capture aleatoric uncertainty, there is a lack of evidence regarding its effectiveness. The literature presents that prediction set size can upper-bound aleatoric uncertainty or that prediction sets are larger for *difficult* instances and smaller for *easy* ones, but a validation of this attribute of conformal predictors is missing. This work investigates how effectively conformal predictors quantify aleatoric uncertainty, specifically the inherent ambiguity in datasets caused by overlapping classes. We perform this by measuring the correlation between prediction set sizes and the number of distinct labels assigned by human annotators per instance. We further assess the similarity between prediction sets and human-provided annotations. We use three conformal prediction approaches to generate prediction sets for eight deep learning models trained on four datasets. The datasets contain annotations from multiple human annotators (ranging from five to fifty participants) per instance, enabling the identification of class overlap. We show that the vast majority of the conformal prediction outputs show a very weak to weak correlation with human annotations, with only a few showing moderate correlation. These findings underscore the necessity of critically reassessing the prediction sets generated using conformal predictors. While they can provide a higher coverage of the true classes, their capability in capturing aleatoric uncertainty remains limited.

1. Introduction

Quantifying model uncertainty is critical for improving model transparency and can enhance the performance of downstream tasks such as active learning and out-of-distribution (OOD) detection [20, 21]. It is usually categorized into aleatoric uncertainty (inherent to the data and irreducible) and epistemic uncertainty (related to model choice and reducible) to satisfy each task’s requirements [8, 14, 17, 30]. For example, in active learning, we would

want to deprioritize samples with high aleatoric and low epistemic uncertainty [22]. Similarly, in OOD detection, we want to avoid confounding previously seen (in-distribution) high aleatoric uncertainty samples with high epistemic uncertainty samples.

Conformal prediction (CP) is a framework for uncertainty quantification that generates prediction sets that are statistically guaranteed to include the true class at a chosen confidence level [26, 36]. This is as opposed to the conventional models that output maximum-likelihood predictions $y \in \mathcal{Y}$. CP is particularly helpful where class distributions overlap and we need to identify all the likely classes and rule out the rest [2].

For a model trained on a dataset $(X_i, Y_i) \in \mathcal{X} \times \mathcal{Y}$ for $i = 1, \dots, n$, CP constructs a prediction set $\mathcal{C}(X_{\text{test}}) \subseteq \mathcal{Y}$ for a test input $(X_{\text{test}}, Y_{\text{test}})$, with the finite-sample guarantee, $\mathbb{P}(Y_{\text{test}} \in \mathcal{C}(X_{\text{test}})) \geq 1 - \alpha$, where $\alpha \in (0, 1)$ is a user-specified target error level.

CP captures aleatoric uncertainty by calibrating prediction sets whose size adapts to the ambiguity in the data, regardless of the underlying model architecture [6, 7, 28]. This ability stems from using a conformity score, often derived from model outputs such as softmax probabilities, whose entropy quantifies aleatoric uncertainty on a per-instance basis [22]. Given class probabilities that are log-concave and that achieve near-perfect calibration, we can assume that the prediction set size, $|\mathcal{C}(X)|$, and an existing aleatoric uncertainty quantification method, softmax entropy [22], are positively correlated. We show evidence of this in the later parts of the paper. Correia et al. [9] also provide theoretical evidence that the prediction set size upper bounds the conditional entropy $H(X|Y)$, which captures the true intrinsic uncertainty in the distribution of labels Y and inputs X . However, there is no clear empirical evidence of how good conformal predictors are at capturing aleatoric uncertainty, or if they do at all. In this work, we aim to address this gap.

Beyond theoretical interest, understanding what prediction set sizes represent is essential for their effective use in downstream tasks, particularly in decision-support systems that involve human interaction. User studies have shown that CP can improve human-AI complementarity in auto-

mated decision-support systems [10, 32, 33]. In such experiments, the size of the prediction sets is assumed to determine the difficulty of a classification task for human participants. In this work, we aim to evaluate this assumption empirically.

Aleatoric uncertainty arises from inherent variability that cannot be resolved through additional data or model refinement [14, 15]. In this work, we specifically focus on aleatoric uncertainty stemming from class overlap, i.e., cases where semantically distinct classes exhibit similar visual or structural characteristics in the input space, rendering accurate classification inherently uncertain. This form of uncertainty is often revealed through human annotation studies, where multiple annotators are tasked with labeling the same instance. When annotators consistently assign multiple distinct labels to a single instance, either individually or across annotators, this pattern suggests the presence of class overlap. It indicates that the resulting uncertainty is not due to noise or labeling error, but rather reflects intrinsic ambiguity in the data itself [19, 35].

To systematically capture this form of instance-level ambiguity, several datasets have been re-annotated—either in whole or in part—with labels from multiple annotators to better reflect human perception and uncertainty [5, 24, 25]. Ambiguous instances are typically characterised by multiple, usually conflicting, labels assigned by different annotators, while non-ambiguous instances often tend to receive similar and consistent annotations [16, 24]. For model training purposes, single labels are often derived via majority voting or by retaining the original labels, whereas the full distribution of annotator labels is preserved in the test set. This allows for a more nuanced evaluation of uncertainty quantification frameworks such as CP, particularly in capturing instance-level ambiguity.

In this paper, we focus on datasets that contain multiple human annotations per instance. This enables us to identify and quantify class overlap as a source of aleatoric uncertainty. We then investigate whether this human-perceived ambiguity correlates with the uncertainty captured by conformal predictors, as reflected in the size of their prediction sets. While annotator disagreement has also been used as a proxy for aleatoric uncertainty [16, 21, 34], we focus on class overlap since we are interested in assessing the prediction sets. We also evaluate the performance of these prediction sets and analyze how their size influences both coverage and the strength of the correlation with class overlap. Additionally, we employ similarity metrics to assess if the prediction sets correctly identify labels collected from the multiple annotators. We define an instance as exhibiting class overlap if it contains two or more distinct class labels from an individual or multiple annotators. The degree of class overlap is quantified by the number of distinct labels assigned to the instance.

The primary contributions of our paper are as follows,

- We evaluate the performance of three CP approaches at capturing aleatoric uncertainty caused by an inherent class overlap in four datasets.
- We show that the employed conformal predictors frequently construct prediction sets that correlate weakly with the dataset’s inherent class overlap.
- We provide empirical evidence that a growing prediction set size does not necessarily result in improved coverage of the true classes, especially in datasets with a large number of categories.
- In addition, we also find that most of the prediction sets substantially differ from human annotations.

2. Related work

Despite achieving high predictive accuracy, deep learning models often produce overconfident softmax probabilities, making them unreliable for uncertainty estimation [13]. In response, a range of model uncertainty quantification methods have been proposed, including Monte Carlo dropout [12], test-time augmentation [3], deep ensembles [18], and evidential deep learning [31]. While effective in some settings, these methods often suffer from architectural constraints and substantial computational overhead [10]. As an alternative, CP offers a model-agnostic approach that mirrors human behavior under uncertainty, providing sets of plausible answers rather than a single maximum-likelihood prediction [26, 36]. These prediction sets adapt in size to reflect the model’s confidence, offering a direct and interpretable measure of uncertainty [6, 7, 28].

Uncertainty quantification methods are commonly evaluated through proxy tasks such as active learning and OOD detection [22]. While useful, these indirect assessments often rely on task-specific assumptions that may not align with the original objective of uncertainty estimation. An alternative is directly evaluating uncertainty estimates on the primary task, e.g., classification, by comparing them to human annotator disagreement [29]. This provides a task-relevant benchmark that more faithfully reflects the intrinsic ambiguity present in the data. In contrast to active learning, which evaluates uncertainty based on its utility for informative sample selection rather than its fidelity to actual data ambiguity, or OOD detection, which relies on model confidence to flag inputs unlike the training data rather than genuine data ambiguity, human annotators’ based evaluation offers a principled target for evaluating uncertainty grounded in the data’s inherent complexity.

While ambiguity in human annotations has been proposed as a benchmark for model uncertainty, conformal predictors are typically assessed solely based on their coverage guarantees, i.e., whether the true class falls within the prediction set [2, 7], without regard to whether their prediction sets align with regions of genuine ambiguity in the

data. Although coverage is central to the CP framework, it does not capture the informativeness of the prediction sets themselves. Despite claims that prediction set size reflects aleatoric uncertainty, this assumption remains largely untested. There is a lack of rigorous evaluations that assess whether variation in prediction set size corresponds meaningfully to inherent data ambiguity.

3. Conformal prediction methods

In multi-class classification, we consider a predictive model $\hat{f} : \mathcal{X} \rightarrow \mathbb{R}^K$ that outputs a confidence vector $\hat{f}(X) \in \mathbb{R}^K$ for each input $X \in \mathcal{X}$, where $\hat{f}(X)_y$ denotes the predicted probability assigned to class $y \in 1, \dots, K$. For a test input x_{test} , we construct a prediction set $\mathcal{C}(x_{\text{test}}) \subseteq 1, \dots, K$ that contains all classes satisfying:

$$\mathcal{C}(x_{\text{test}}) = \left\{ y \in 1, \dots, K : \hat{f}(x_{\text{test}})_y \geq 1 - \hat{q} \right\}, \quad (1)$$

where \hat{q} is a threshold computed from a calibration set $(X_{\text{cal}}, Y_{\text{cal}})$ under the assumption that the calibration and test sets are exchangeable.

We use three CP approaches to generate prediction sets: the least ambiguous set-valued classifier (LAC) [28], adaptive prediction sets (APS) [26], and regularized adaptive prediction sets (RAPS) [2]. They are introduced next.

Least Ambiguous Set-Valued Classifier The Least Ambiguous Classifier (LAC) defines a score function,

$$s(x, y) = 1 - \hat{f}(x)_y, \quad (2)$$

where $\hat{f}(x)_y$ is the softmax probability assigned to the true class y . For a calibration set of size n and target error rate α , the $(1 - \alpha)$ quantile is computed applying a finite-sample correction:

$$\hat{q} = \text{quantile} \left(\{s_1, \dots, s_n\}; \frac{[(1 - \alpha)(n + 1)]}{n} \right), \quad (3)$$

The prediction set is then constructed:

$$\mathcal{C}(x_{\text{test}}) = \left\{ y : \hat{f}(x_{\text{test}})_y \geq 1 - \hat{q} \right\} \quad (4)$$

Because it only considers the true class probability during calibration, LAC can yield empty prediction sets for high-uncertainty inputs.

Adaptive Prediction Sets Adaptive Prediction Sets (APS) sort the softmax outputs in descending order to obtain $\pi(x)$. The conformity score is the cumulative probability up to the true class index:

$$s(x, y) = \sum_{j=1}^k \hat{f}(x)_{\pi_j(x)}, \quad (5)$$

where $\pi_k(x) = y$ and k is the index of true class. Using the same quantile computation procedure as in LAC, the prediction set is given by:

$$\begin{aligned} \mathcal{C}(x_{\text{test}}) &= \{\pi_1, \dots, \pi_k\}, \\ k &= \inf \left\{ k : \sum_{j=1}^k \hat{f}(x_{\text{test}})_{\pi_j} \geq \hat{q} \right\}. \end{aligned} \quad (6)$$

By summing over multiple class probabilities, APS avoids the empty prediction set issue observed in LAC.

Regularized Adaptive Prediction Sets RAPS augments APS with a regularization term that encourages prediction sets to reflect model confidence, while maintaining coverage. The conformity score is defined as:

$$s(x, y) = \sum_{j=1}^k \hat{f}(x)_{\pi_j} + \lambda(k - k_{\text{reg}}), \quad (7)$$

where $\pi_k = y$, and k_{reg} is a target prediction set size. Following Angelopoulos et al. [2], we tune the regularization parameter λ on a held-out 20% subset of the calibration set, selecting from the grid $\{0.001, 0.01, 0.1, 0.2, 0.5\}$. This procedure yielded $\lambda = 0.1$ for all datasets, and we set the regularization parameter $k_{\text{reg}} = 1$.

After computing the quantile \hat{q} as in LAC, the prediction set is constructed as:

$$\begin{aligned} \mathcal{C}(x_{\text{test}}) &= \{\pi_1, \dots, \pi_k\}, \\ k &= \inf \left\{ k : \sum_{j=1}^k \hat{f}(x_{\text{test}})_{\pi_j} + \lambda(k - k_{\text{reg}}) \geq \hat{q} \right\}. \end{aligned} \quad (8)$$

4. Experiments

4.1. Datasets

The datasets used in our experiments are introduced next, with their corresponding count of distinct human labels distribution shown in Figure 1. The average number of human annotators per instance is also reported when available in the datasets. For all the datasets, the calibration sets are selected from the same distribution as the test set.

CIFAR-10H [24] is a collection of 511,400 human categorizations for the 10,000 images in the test subset of the

CIFAR-10 dataset. We use 1,000 uniformly sampled instances from the original CIFAR-10 test set as a calibration set, with the remainder used for evaluation. An average of 50.09 annotators labelled each image in the test set, and class overlap exists in 56.2% of these images.

MLRSNet [25] contains 46 categories. It contains 109,161 images, and labels are collected from 50 human annotators. We use 9,200 images, selected uniformly across all categories, as a calibration set, and 20,000 images as a test set. There is class overlap in 97.2% of the test images.

FER+ [4] is a version of the facial expression recognition (FER) dataset [11] that contains facial images and their corresponding single labels from seven categories. FER+ incorporates annotations from multiple human participants for each facial image. The dataset includes a training set of 28,709 images, and a public and private test set, each containing 3,589 images. We use the public and private test sets as calibration and test sets, respectively. On average, 9.35 annotators labelled the test images. Class overlap exists in 69.8% of the test set images.

ImageNet-Real [5] is constructed by re-annotating the ImageNet validation set [27], with each instance labeled by five human annotators. Each annotator is provided with eight candidate labels and asked whether each label is present in an image, setting the maximum number of labels for an image to eight. 15.8% of the images received overlapping classes. After excluding images with missing labels, we selected 20,000 images from the validation set as the calibration set and 26,000 as the test set, ensuring a uniform distribution across all categories.

For each dataset, we searched for the best target error value $\alpha \in \{0.05, 0.1, 0.15, 0.2\}$ that minimizes the ratio of the CP mean set size to coverage. This ensures high coverage while keeping the prediction sets concise and informative. Apart from the ImageNet-Real dataset, which resulted in an $\alpha = 0.10$, the rest of the datasets led to $\alpha = 0.05$.

4.2. Models

We used eight deep learning architecture: ResNet18, ResNet34, ResNet50, Vgg16, Vgg19, DenseNet121, DenseNet161, and MobileNet-v2.¹ All models were trained from scratch using an Adam optimizer with a decaying learning rate of 1e-4 and a categorical cross-entropy loss.

4.3. Evaluation

We compute Expected Calibration Error (ECE) [13, 23] to measure model calibration. ECE assesses the reliability of softmax outputs employed in constructing prediction sets.

¹<https://pytorch.org/vision/main/models.html>

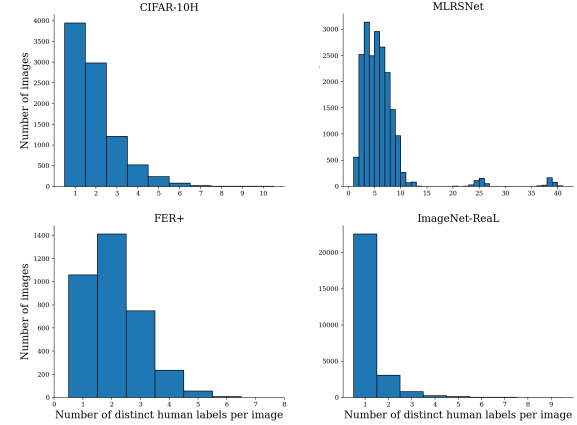


Figure 1. Distinct human labels distribution in the CIFAR-10H, MLRSNet, FER+, and ImageNet-Real datasets. The X-axis shows the number of distinct human labels per image, and the Y-axis shows the number of images.

Lower ECE values indicate better calibration, with ECE=0 indicating perfect calibration and ECE=1 indicating maximum miscalibration. ECE first partitions predictions into M equally spaced bins, B , and takes a weighted average of the difference between accuracy and confidence. It is computed as follows for n instances.

$$\text{ECE} = \sum_{m=1}^M \frac{|B_m|}{n} |\text{acc}(B_m) - \text{conf}(B_m)| \quad (9)$$

We evaluate the performance of the conformal predictors using coverage, size-stratified coverage (SSC) [1], and mean prediction set size (\bar{w}). Coverage measures the ratio of the presence of the true class, y , in a prediction set, $\mathcal{C}(x)$, as follows,

$$\text{Coverage} = \frac{1}{N} \sum_{i=1}^N \mathbb{1} \{y_i \in \mathcal{C}(x_i)\} \quad (10)$$

SSC first discretizes the prediction set into g bins based on set size and then computes the worst case coverage among all bins as follows,

$$\text{SSC} = \min_{g \in \{1, \dots, G\}} \frac{1}{|I_g|} \sum_{i \in I_g} \mathbb{1} \{y_i \in \mathcal{C}(x_i)\} \quad (11)$$

where I_g is a group of sets that belong to the g^{th} size group, and G is the number of distinct size groups. Mean set size assesses the capability of conformal predictors in generating concise sets. It is computed as, $\bar{w} = \frac{1}{N} \sum_{i=1}^N |\mathcal{C}(x_i)|$.

We use Spearman’s rank correlation coefficient (r_s) to assess the correlation between the prediction set size and the class overlap or the number of distinct human labels. We assess the similarity between the prediction sets and

human annotations using the similarity metrics precision, recall, subset-accuracy, and hamming loss. Instances with empty prediction sets are excluded from the correlation and similarity analysis.

5. Results

5.1. Expected Calibration Error

Table 1 presents the ECE using M=15 bins for all the models. The majority of models exhibit strong calibration with a median ECE of 0.024 across all experiments. The Vgg16 and Vgg19 models show the highest degree of miscalibration on the MLRSNet dataset.

5.2. Conformal predictors' performance

The models' and conformal predictors' performance on all the four datasets is shown in Tables 2-5. We report the models' accuracy and the conformal predictors' coverage, SSC, and mean set size (\bar{w}). The APS and RAPS methods consistently outperform the LAC method in covering the true class at the cost of a larger mean set size.

Notably, Vgg16 and Vgg19, which show high miscalibration on the MLRSNet dataset, also achieve lower accuracy (Table 3). Although their coverage under the LAC method is comparable to that of other models, they are consistently outperformed when using the APS and RAPS methods.

While this trend is less apparent on datasets with similar model accuracies, we observe that lower-accuracy models consistently yield larger mean prediction set sizes across all methods. This pattern is evident for VGG16, VGG19, and MobileNet-v2 on the MLRSNet dataset (Table 3), and similarly for ResNet18, VGG16, VGG19, and MobileNet-v2 on the ImageNet-ReaL dataset (Table 5).

LAC frequently generates smaller set sizes. This can be seen in Tables 2-5. LAC can also lead to empty prediction sets, as is especially the case for the models trained on the CIFAR-10H, MLRSNet, and ImageNet-Real datasets (See the distribution of the prediction set sizes in Figure A1 in the Appendix).

Conformal prediction sets constructed with the ResNet18 model for sample images from all datasets are shown in Figure 2. As shown in the figure, while all approaches successfully cover the true class, their performance at capturing the human annotation ambiguity varies and is usually limited.

5.3. Coverage at different prediction set sizes

Larger prediction sets do not always lead to improved coverage (We show how coverage changes with increasing set sizes in Figure A2 in the Appendix). This is especially the case for the datasets with a large number of categories, MLRSNet (46 categories) and ImageNet-Real (1000 cat-

egories). However, some of the models trained on the CIFAR-10H and FER+ datasets led to better coverage with increasing set size.

5.4. Correlation analysis

The Spearman's r_s between prediction set sizes and class overlap is presented in Table 6, and the Spearman's r_s between the prediction set sizes and softmax entropy is shown in Table 7. We observe that Spearman's r_s between prediction set size and class overlap is usually weak to very weak, with only a few showing a moderate correlation, indicating limited alignment of the prediction sets with human-perceived ambiguity. In contrast, as we expected, prediction set size usually exhibits a strong to very strong Spearman's r_s with softmax entropy.

An increased prevalence of larger prediction sets is associated with an improved Spearman's r_s with class overlap, suggesting that prediction set size positively contributes to capturing instance-level ambiguity (See Figure A3 in the Appendix).

5.5. Similarity analysis

All methods achieve low subset-accuracy and relatively higher Hamming loss, showing the substantial difference between prediction sets and human annotations. Precision and recall are influenced by prediction set size and the number of distinct human labels. Smaller prediction sets and more diverse human annotations, such as CIFAR-10H, MLRSNet, and FER+, yield higher precision. In contrast, ImageNet-ReaL exhibits lower precision and higher recall due to fewer human labels (five annotators chose from eight labels). Tabular results of our similarity analysis are presented in Tables A1 to A4 in the Appendix.

6. Discussion

We evaluate the common assumption that conformal predictors capture aleatoric uncertainty. We perform this by measuring their correlation and similarity with the ambiguity present in human annotations across four datasets. Our experiments use a diverse set of datasets with varying degrees of class overlap from human annotators. Overall, we found that conformal predictors find it challenging to capture the class overlap recorded using multiple human annotators.

In agreement with previous works [2], we see that the conformal predictors lead to an increased coverage of the true class for all the datasets and models. This is presented in Tables 2-5.

Even though conformal predictors often show a strong correlation with aleatoric uncertainty quantifiers such as the softmax entropy (See Table 7), they usually fail to capture the inherent class overlap in the employed datasets and show substantial differences from human annotations. For

Table 1. Expected Calibration Error (ECE) with M = 15 bins.

| Models | CIFAR-10H | MLRSNet | FER+ | ImageNet-ReAL |
|--------------|-----------|---------|-------|---------------|
| ResNet18 | 0.021 | 0.013 | 0.032 | 0.021 |
| ResNet34 | 0.026 | 0.023 | 0.035 | 0.027 |
| ResNet50 | 0.023 | 0.030 | 0.026 | 0.032 |
| Vgg16 | 0.016 | 0.100 | 0.037 | 0.020 |
| Vgg19 | 0.022 | 0.119 | 0.053 | 0.020 |
| DenseNet121 | 0.020 | 0.018 | 0.034 | 0.020 |
| DenseNet161 | 0.021 | 0.019 | 0.038 | 0.047 |
| MobileNet-v2 | 0.025 | 0.012 | 0.027 | 0.020 |

Table 2. Models' and conformal predictors' performance on the CIFAR-10H dataset.

| Models | Accuracy | LAC | | | APS | | | RAPS | | |
|--------------|----------|----------|-------|-----------|----------|-------|-----------|----------|-------|-----------|
| | | Coverage | SSC | \bar{w} | Coverage | SSC | \bar{w} | Coverage | SSC | \bar{w} |
| ResNet18 | 0.930 | 0.944 | 0.894 | 1.040 | 0.977 | 0.953 | 1.357 | 0.978 | 0.952 | 1.361 |
| ResNet34 | 0.933 | 0.953 | 0.833 | 1.062 | 0.979 | 0.953 | 1.369 | 0.976 | 0.950 | 1.304 |
| ResNet50 | 0.936 | 0.953 | 0.500 | 1.050 | 0.974 | 0.939 | 1.263 | 0.975 | 0.959 | 1.285 |
| Vgg16 | 0.941 | 0.955 | 0.853 | 1.049 | 0.982 | 0.930 | 1.328 | 0.979 | 0.882 | 1.263 |
| Vgg19 | 0.939 | 0.951 | 0.000 | 1.039 | 0.976 | 0.907 | 1.264 | 0.973 | 0.895 | 1.207 |
| DenseNet121 | 0.940 | 0.942 | 0.000 | 1.006 | 0.979 | 0.938 | 1.395 | 0.975 | 0.947 | 1.274 |
| DenseNet161 | 0.940 | 0.944 | 0.000 | 1.011 | 0.977 | 0.941 | 1.347 | 0.976 | 0.927 | 1.309 |
| MobileNet-v2 | 0.939 | 0.951 | 0.000 | 1.030 | 0.984 | 0.953 | 1.425 | 0.982 | 0.966 | 1.370 |

Table 3. Models' and conformal predictors' performance on the MLRSNet dataset.

| Models | Accuracy | LAC | | | APS | | | RAPS | | |
|--------------|----------|----------|-------|-----------|----------|-------|-----------|----------|-------|-----------|
| | | Coverage | SSC | \bar{w} | Coverage | SSC | \bar{w} | Coverage | SSC | \bar{w} |
| ResNet18 | 0.927 | 0.951 | 0.000 | 1.081 | 0.984 | 0.889 | 1.575 | 0.985 | 0.900 | 1.624 |
| ResNet34 | 0.923 | 0.951 | 0.831 | 1.090 | 0.982 | 0.500 | 1.500 | 0.982 | 0.750 | 1.526 |
| ResNet50 | 0.918 | 0.949 | 0.780 | 1.113 | 0.978 | 0.667 | 1.504 | 0.978 | 0.667 | 1.508 |
| Vgg16 | 0.872 | 0.950 | 0.750 | 1.613 | 0.955 | 0.833 | 1.798 | 0.963 | 0.887 | 2.059 |
| Vgg19 | 0.844 | 0.955 | 0.889 | 2.106 | 0.958 | 0.875 | 2.352 | 0.974 | 0.953 | 3.386 |
| DenseNet121 | 0.933 | 0.951 | 0.000 | 1.059 | 0.984 | 0.000 | 1.513 | 0.985 | 0.500 | 1.547 |
| DenseNet161 | 0.946 | 0.956 | 0.000 | 1.026 | 0.985 | 0.928 | 1.320 | 0.984 | 0.905 | 1.316 |
| MobileNet-v2 | 0.860 | 0.953 | 0.750 | 1.635 | 0.978 | 0.937 | 2.596 | 0.981 | 0.917 | 2.859 |

the challenging dataset, MLRSNet, where 97.2% of the images have overlapping classes (or received more than two distinct human labels), the Spearman's r_s between the prediction set size and class overlap was always very weak. This highlights the particular shortcomings of prediction

sets when presented with challenging tasks. We observe weak and a few moderate correlations in cases where class overlap is low, as in the ImageNet-Real dataset (there is class overlap in only 15.8% of the total images from the ImageNet-ReAL dataset) or where the number of categories

Table 4. Models’ and conformal predictors’ performance on the FER+ dataset.

| Models | Accuracy | LAC | | | APS | | | RAPS | | |
|--------------|----------|----------|-------|-----------|----------|-------|-----------|----------|-------|-----------|
| | | Coverage | SSC | \bar{w} | Coverage | SSC | \bar{w} | Coverage | SSC | \bar{w} |
| ResNet18 | 0.825 | 0.941 | 0.818 | 1.561 | 0.961 | 0.920 | 2.250 | 0.960 | 0.920 | 2.233 |
| ResNet34 | 0.839 | 0.939 | 0.934 | 1.484 | 0.958 | 0.936 | 2.085 | 0.958 | 0.933 | 2.138 |
| ResNet50 | 0.838 | 0.940 | 0.857 | 1.493 | 0.959 | 0.800 | 2.027 | 0.961 | 0.857 | 2.148 |
| Vgg16 | 0.835 | 0.946 | 0.875 | 1.530 | 0.970 | 0.952 | 2.274 | 0.970 | 0.951 | 2.318 |
| Vgg19 | 0.823 | 0.943 | 0.935 | 1.561 | 0.964 | 0.875 | 2.222 | 0.966 | 0.923 | 2.316 |
| DenseNet121 | 0.832 | 0.945 | 0.833 | 1.521 | 0.965 | 0.833 | 2.199 | 0.967 | 0.857 | 2.273 |
| DenseNet161 | 0.836 | 0.943 | 0.938 | 1.496 | 0.962 | 0.932 | 2.208 | 0.964 | 0.929 | 2.283 |
| MobileNet-v2 | 0.827 | 0.944 | 0.940 | 1.563 | 0.965 | 0.952 | 2.237 | 0.966 | 0.952 | 2.311 |

Table 5. Models’ and conformal predictors’ performance on the ImageNet-ReaL dataset.

| Models | Accuracy | LAC | | | APS | | | RAPS | | |
|--------------|----------|----------|-------|-----------|----------|-------|-----------|----------|-------|-----------|
| | | Coverage | SSC | \bar{w} | Coverage | SSC | \bar{w} | Coverage | SSC | \bar{w} |
| ResNet18 | 0.725 | 0.902 | 0.500 | 2.994 | 0.939 | 0.000 | 12.680 | 0.939 | 0.000 | 12.712 |
| ResNet34 | 0.759 | 0.899 | 0.681 | 2.157 | 0.940 | 0.000 | 8.894 | 0.940 | 0.500 | 8.943 |
| ResNet50 | 0.785 | 0.903 | 0.000 | 1.760 | 0.946 | 0.000 | 7.768 | 0.946 | 0.000 | 7.892 |
| Vgg16 | 0.745 | 0.902 | 0.000 | 2.461 | 0.943 | 0.000 | 10.690 | 0.943 | 0.000 | 10.587 |
| Vgg19 | 0.751 | 0.903 | 0.000 | 2.355 | 0.946 | 0.000 | 10.764 | 0.946 | 0.000 | 10.692 |
| DenseNet121 | 0.770 | 0.902 | 0.000 | 2.030 | 0.946 | 0.000 | 8.644 | 0.946 | 0.000 | 8.702 |
| DenseNet161 | 0.796 | 0.902 | 0.000 | 1.633 | 0.942 | 0.000 | 6.053 | 0.942 | 0.000 | 6.034 |
| MobileNet-v2 | 0.744 | 0.902 | 0.688 | 2.496 | 0.940 | 0.000 | 9.539 | 0.941 | 0.000 | 9.730 |

is small as in the FER+ dataset (the FER+ has only seven categories, which is the lowest number of categories relative to the rest of the datasets).

7. Conclusion

This work provides the first empirical evaluation of conformal predictors’ ability at quantifying aleatoric uncertainty arising from class overlap. To probe this capability, we used fitting datasets whose inherent ambiguity was identified by collecting labels from multiple annotators (ranging between five and fifty participants) per single instance. We applied three conformal prediction methods across four datasets exhibiting varying degrees of class overlap. Our findings indicate that the Spearman’s r_s between conformal prediction set uncertainty, measured by prediction set size, and class overlap, measured by the number of distinct human labels, was frequently in the very weak to weak range. These results suggest that conformal predictors, while offering valid coverage, often fail to reflect the underlying ambiguity in data caused by class overlap. We also observed

that the correlation between prediction set size and class overlap improves with the prevalence of larger prediction sets. While we hypothesized that increasing set size would consistently enhance coverage or the likelihood of including the true class, this expectation did not hold across most of our experiments. These findings underscore that prediction set size should not be uncritically interpreted as a proxy for aleatoric uncertainty, particularly in the presence of inherent labeling ambiguity. This paper focuses on aleatoric uncertainty arising from class overlap. Although other sources of aleatoric uncertainty, such as intra-class variability or label noise, are often intertwined with class overlap, they are not explicitly addressed in this work and are left for future investigation.

Acknowledgments

This work was partially supported by the Wallenberg AI, Autonomous Systems and Software Program (WASP) funded by the Knut and Alice Wallenberg Foundation.

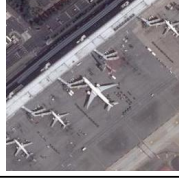
| | | | | |
|-----------------------|---|---|---|--|
| |  |  |  |  |
| Distinct human labels | airplane, bird, cat, dog | airplane, airport, buildings, cars, pavement, trees | neutral, sadness | European fire salamander, American chameleon, frilled lizard |
| Test label | bird | airplane | sadness | European fire salamander |
| LAC | bird | airplane, railway station | neutral, sadness | European fire salamander, box turtle, green lizard |
| APS | bird | airplane, railway station | neutral, sadness, disgust | European fire salamander, box turtle, green lizard, banded gecko, American chameleon |
| RAPS | bird | airplane, railway station | neutral, sadness, disgust | European fire salamander, box turtle, green lizard, banded gecko, American chameleon |

Figure 2. Conformal prediction set outputs for sample images from the four datasets. Columns from left to right: CIFAR-10H (leftmost), MLRSNet, FER+, and ImageNet-Real (rightmost).

Table 6. Spearman’s rank correlation coefficient, r_s , $p < .001$, between conformal prediction set sizes and class overlap.

| Models | CIFAR-10H | | | MLRSNet | | | FER+ | | | ImageNet-Real | | |
|--------------|-----------|-------|-------|---------|--------|--------|-------|-------|-------|---------------|-------|-------|
| | LAC | APS | RAPS | LAC | APS | RAPS | LAC | APS | RAPS | LAC | APS | RAPS |
| ResNet18 | 0.131 | 0.231 | 0.231 | 0.045 | 0.064 | 0.064 | 0.365 | 0.325 | 0.326 | 0.320 | 0.316 | 0.316 |
| ResNet34 | 0.125 | 0.209 | 0.199 | 0.020 | 0.051 | 0.052 | 0.363 | 0.240 | 0.232 | 0.353 | 0.355 | 0.355 |
| ResNet50 | 0.144 | 0.215 | 0.219 | 0.038 | 0.049 | 0.050 | 0.364 | 0.302 | 0.280 | 0.361 | 0.364 | 0.364 |
| Vgg16 | 0.137 | 0.230 | 0.220 | -0.010 | -0.016 | -0.025 | 0.409 | 0.277 | 0.268 | 0.344 | 0.347 | 0.347 |
| Vgg19 | 0.148 | 0.222 | 0.215 | 0.006 | 0.007 | -0.003 | 0.390 | 0.265 | 0.252 | 0.352 | 0.349 | 0.349 |
| DenseNet121 | 0.018 | 0.221 | 0.204 | 0.037 | 0.058 | 0.058 | 0.393 | 0.177 | 0.168 | 0.351 | 0.357 | 0.357 |
| DenseNet161 | 0.056 | 0.201 | 0.196 | 0.023 | 0.037 | 0.037 | 0.402 | 0.253 | 0.237 | 0.348 | 0.355 | 0.355 |
| MobileNet-v2 | 0.109 | 0.256 | 0.248 | 0.060 | 0.064 | 0.066 | 0.374 | 0.315 | 0.307 | 0.332 | 0.331 | 0.331 |

Table 7. Spearman’s rank correlation coefficient, r_s , $p < .001$, between conformal prediction set sizes and softmax entropy.

| Models | CIFAR-10H | | | MLRSNet | | | FER+ | | | ImageNet-Real | | |
|--------------|-----------|-------|-------|---------|-------|-------|-------|-------|-------|---------------|-------|-------|
| | LAC | APS | RAPS | LAC | APS | RAPS | LAC | APS | RAPS | LAC | APS | RAPS |
| ResNet18 | 0.326 | 0.614 | 0.614 | 0.432 | 0.723 | 0.733 | 0.824 | 0.935 | 0.934 | 0.924 | 0.953 | 0.953 |
| ResNet34 | 0.391 | 0.595 | 0.573 | 0.461 | 0.706 | 0.712 | 0.785 | 0.918 | 0.916 | 0.881 | 0.932 | 0.933 |
| ResNet50 | 0.359 | 0.547 | 0.558 | 0.505 | 0.719 | 0.720 | 0.804 | 0.912 | 0.903 | 0.828 | 0.909 | 0.910 |
| Vgg16 | 0.361 | 0.583 | 0.561 | 0.731 | 0.746 | 0.776 | 0.804 | 0.902 | 0.898 | 0.898 | 0.943 | 0.942 |
| Vgg19 | 0.324 | 0.551 | 0.519 | 0.814 | 0.820 | 0.860 | 0.800 | 0.917 | 0.911 | 0.892 | 0.940 | 0.939 |
| DenseNet121 | 0.091 | 0.571 | 0.523 | 0.378 | 0.675 | 0.683 | 0.790 | 0.885 | 0.877 | 0.862 | 0.932 | 0.932 |
| DenseNet161 | 0.157 | 0.536 | 0.521 | 0.253 | 0.615 | 0.613 | 0.790 | 0.876 | 0.863 | 0.814 | 0.898 | 0.897 |
| MobileNet-v2 | 0.283 | 0.614 | 0.593 | 0.819 | 0.892 | 0.903 | 0.828 | 0.930 | 0.930 | 0.903 | 0.943 | 0.944 |

References

- [1] Anastasios N Angelopoulos and Stephen Bates. A gentle introduction to conformal prediction and distribution-free uncertainty quantification. *arXiv preprint arXiv:2107.07511*, 2021. [4](#)
- [2] Anastasios Nikolas Angelopoulos, Stephen Bates, Michael Jordan, and Jitendra Malik. Uncertainty sets for image classifiers using conformal prediction. In *International Conference on Learning Representations*, 2021. [1, 2, 3, 5](#)
- [3] Murat Seckin Ayhan and Philipp Berens. Test-time data augmentation for estimation of heteroscedastic aleatoric uncertainty in deep neural networks. In *Medical Imaging with Deep Learning*, 2018. [2](#)
- [4] Emad Barsoum, Cha Zhang, Cristian Canton Ferrer, and Zhengyou Zhang. Training deep networks for facial expression recognition with crowd-sourced label distribution. In *ACM International Conference on Multimodal Interaction (ICMI)*, 2016. [4](#)
- [5] Lucas Beyer, Olivier J Hénaff, Alexander Kolesnikov, Xiaohua Zhai, and Aäron van den Oord. Are we done with imagenet? *arXiv preprint arXiv:2006.07159*, 2020. [2, 4](#)
- [6] Luben Cabezas, Wagner S Santos, Thiago R Ramos, and Rafael Izbicki. Epistemic uncertainty in conformal scores: A unified approach. *arXiv preprint arXiv:2502.06995*, 2025. [1, 2](#)
- [7] Christopher Clark, Scott Kinder, Didem Egemen, Brian Befano, Kanan Desai, Syed Rakin Ahmed, Praveer Singh, Ana Cecilia Rodriguez, Jose Jeronimo, Silvia De Sanjose, et al. Conformal prediction and monte carlo inference for addressing uncertainty in cervical cancer screening. In *International Workshop on Uncertainty for Safe Utilization of Machine Learning in Medical Imaging*, pages 205–214. Springer, 2024. [1, 2](#)
- [8] Mathieu Cocheteux, Julien Moreau, and Franck Davoine. Uncertainty-aware online extrinsic calibration: A conformal prediction approach. In *2025 IEEE/CVF Winter Conference on Applications of Computer Vision (WACV)*, pages 6167–6176. IEEE, 2025. [1](#)
- [9] Alvaro Correia, Fabio Valerio Massoli, Christos Louizos, and Arash Behboodi. An information theoretic perspective on conformal prediction. *Advances in Neural Information Processing Systems*, 37:101000–101041, 2024. [1](#)
- [10] Jesse C Cresswell, Yi Sui, Bhargava Kumar, and Noël Voultis. Conformal prediction sets improve human decision making. In *International Conference on Machine Learning*, pages 9439–9457. PMLR, 2024. [2](#)
- [11] Will Cukierski Dumitru, Ian Goodfellow and Yoshua Bengio. Challenges in representation learning: Facial expression recognition challenge. <https://kaggle.com/competitions/challenges-in-representation-learning-facial-expression-recognition-challenge>, 2013. Kaggle. [4](#)
- [12] Yarin Gal and Zoubin Ghahramani. Dropout as a bayesian approximation: Representing model uncertainty in deep learning. In *international conference on machine learning*, pages 1050–1059. PMLR, 2016. [2](#)
- [13] Chuan Guo, Geoff Pleiss, Yu Sun, and Kilian Q Weinberger. On calibration of modern neural networks. In *International conference on machine learning*, pages 1321–1330. PMLR, 2017. [2, 4](#)
- [14] Eyke Hüllermeier and Willem Waegeman. Aleatoric and epistemic uncertainty in machine learning: An introduction to concepts and methods. *Machine learning*, 110(3):457–506, 2021. [1, 2](#)
- [15] Alex Kendall and Yarin Gal. What uncertainties do we need in bayesian deep learning for computer vision? *Advances in Neural Information Processing Systems*, 30, 2017. [2](#)
- [16] Michael Kirchhof, Enkelejda Kasneci, and Seong Joon Oh. Probabilistic contrastive learning recovers the correct aleatoric uncertainty of ambiguous inputs. In *International Conference on Machine Learning*, pages 17085–17104. PMLR, 2023. [2](#)
- [17] Sergey Korchagin, Ekaterina Zaychenkova, Aleksei Khalin, Aleksandr Yugay, Alexey Zaytsev, and Egor Ershov. Improving uncertainty estimation with confidence-aware training data. In *2025 IEEE/CVF Winter Conference on Applications of Computer Vision (WACV)*, pages 7991–8001. IEEE Computer Society, 2025. [1](#)
- [18] Balaji Lakshminarayanan, Alexander Pritzel, and Charles Blundell. Simple and scalable predictive uncertainty estimation using deep ensembles. *Advances in neural information processing systems*, 30, 2017. [2](#)
- [19] Marian Marchal, Merel Scholman, Frances Yung, and Vera Demberg. Establishing annotation quality in multi-label annotations. In *Proceedings of the 29th International Conference on Computational Linguistics*, pages 3659–3668, 2022. [2](#)
- [20] Bálint Mucsányi, Michael Kirchhof, Elisa Nguyen, Alexander Rubinstein, and Seong Joon Oh. Trustworthy machine learning. *arXiv preprint arXiv:2310.08215*, 2023. [1](#)
- [21] Bálint Mucsányi, Michael Kirchhof, and Seong Joon Oh. Benchmarking uncertainty disentanglement: Specialized uncertainties for specialized tasks. *Advances in Neural Information Processing Systems*, 37:50972–51038, 2024. [1, 2](#)
- [22] Jishnu Mukhoti, Andreas Kirsch, Joost van Amersfoort, Philip HS Torr, and Yarin Gal. Deep deterministic uncertainty: A new simple baseline. In *Proceedings of the IEEE/CVF Conference on Computer Vision and Pattern Recognition*, pages 24384–24394, 2023. [1, 2](#)
- [23] Mahdi Pakdaman Naeini, Gregory Cooper, and Milos Hauskrecht. Obtaining well calibrated probabilities using bayesian binning. In *Proceedings of the AAAI conference on artificial intelligence*, 2015. [4](#)
- [24] Joshua C Peterson, Ruaireidh M Battleday, Thomas L Griffiths, and Olga Russakovsky. Human uncertainty makes classification more robust. In *Proceedings of the IEEE/CVF International Conference on Computer Vision*, pages 9617–9626, 2019. [2, 3](#)
- [25] Xiaoman Qi, Panpan Zhu, Yuebin Wang, Liqiang Zhang, Junhuan Peng, Mengfan Wu, Jialong Chen, Xudong Zhao, Ning Zang, and P Takis Mathiopoulos. Mlrnet: A multi-label high spatial resolution remote sensing dataset for semantic scene understanding. *ISPRS Journal of Photogrammetry and Remote Sensing*, 169:337–350, 2020. [2, 4](#)

[26] Yaniv Romano, Matteo Sesia, and Emmanuel Candes. Classification with valid and adaptive coverage. *Advances in Neural Information Processing Systems*, 33:3581–3591, 2020. [1](#), [2](#), [3](#)

[27] Olga Russakovsky, Jia Deng, Hao Su, Jonathan Krause, Sanjeev Satheesh, Sean Ma, Zhiheng Huang, Andrej Karpathy, Aditya Khosla, Michael Bernstein, et al. Imagenet large scale visual recognition challenge. *International Journal of Computer Vision*, 115:211–252, 2015. [4](#)

[28] Mauricio Sadinle, Jing Lei, and Larry Wasserman. Least ambiguous set-valued classifiers with bounded error levels. *Journal of the American Statistical Association*, 114(525): 223–234, 2019. [1](#), [2](#), [3](#)

[29] Oliver Schrüfer, Manuel Milling, Felix Burkhardt, Florian Eyben, and Björn Schuller. Are you sure? analysing uncertainty quantification approaches for real-world speech emotion recognition. *arXiv preprint arXiv:2407.01143*, 2024. [2](#)

[30] Robin Senge, Stefan Bösner, Krzysztof Dembczyński, Jörg Haasenritter, Oliver Hirsch, Norbert Donner-Banzhoff, and Eyke Hüllermeier. Reliable classification: Learning classifiers that distinguish aleatoric and epistemic uncertainty. *Information Sciences*, 255:16–29, 2014. [1](#)

[31] Murat Sensoy, Lance Kaplan, and Melih Kandemir. Evidential deep learning to quantify classification uncertainty. *Advances in Neural Information Processing Systems*, 31, 2018. [2](#)

[32] Eleni Straitouri and Manuel Gomez Rodriguez. Designing decision support systems using counterfactual prediction sets. In *International Conference on Machine Learning*, pages 46722–46744, 2024. [2](#)

[33] Eleni Straitouri, Lequn Wang, Nastaran Okati, and Manuel Gomez Rodriguez. Improving expert predictions with conformal prediction. In *International Conference on Machine Learning*, pages 32633–32653. PMLR, 2023. [2](#)

[34] D. Tran, J. Z. Liu, M. W. Dusenberry, D. Phan, M. Collier, J. Ren, K. Han, Z. Wang, Z. E. Mariet, H. Hu, N. Band, T. G. J. Rudner, Z. Nado, J. van Amersfoort, A. Kirsch, R. Jenatton, N. Thain, E. K. Buchanan, K. P. Murphy, D. Sculley, Y. Gal, Z. Ghahramani, J. Snoek, and B. Lakshminarayanan. Plex: Towards Reliability Using Pretrained Large Model Extensions. In *First Workshop on Pre-training: Perspectives, Pitfalls, and Paths Forward at ICML*, 2022. [2](#)

[35] Alexandra Uma, Dina Almanea, and Massimo Poesio. Scaling and disagreements: Bias, noise, and ambiguity. *Frontiers in Artificial Intelligence*, 5:818451, 2022. [2](#)

[36] Vladimir Vovk, Alexander Gammerman, and Glenn Shafer. *Algorithmic learning in a random world*. Springer, 2005. [1](#), [2](#)

Appendix

Distribution of prediction set sizes Figure A1 shows the prediction set size distribution of the three conformal predictors.

Coverage at different prediction set sizes We show how coverage changes with increasing set sizes in Figure A2.

Impact of prevalence of larger prediction set sizes on correlation analysis We show how the correlation between prediction set sizes and class overlap changes with the prevalence of larger set sizes in Figure A3. We follow an incremental approach to see the effect of larger set sizes on the correlation analysis. We start with prediction sets with size ≤ 2 and incrementally add sets with larger sizes. The Spearman's rank correlation coefficient of prediction sets that contain larger set sizes shows improvement, albeit small.

Similarity between conformal prediction sets and human annotation We assess the similarity between the prediction sets of the conformal predictors and human annotations using the metrics precision, recall, subset-accuracy (S. Acc), and hamming loss. The results on all the datasets are presented in Tables A1 to A4.

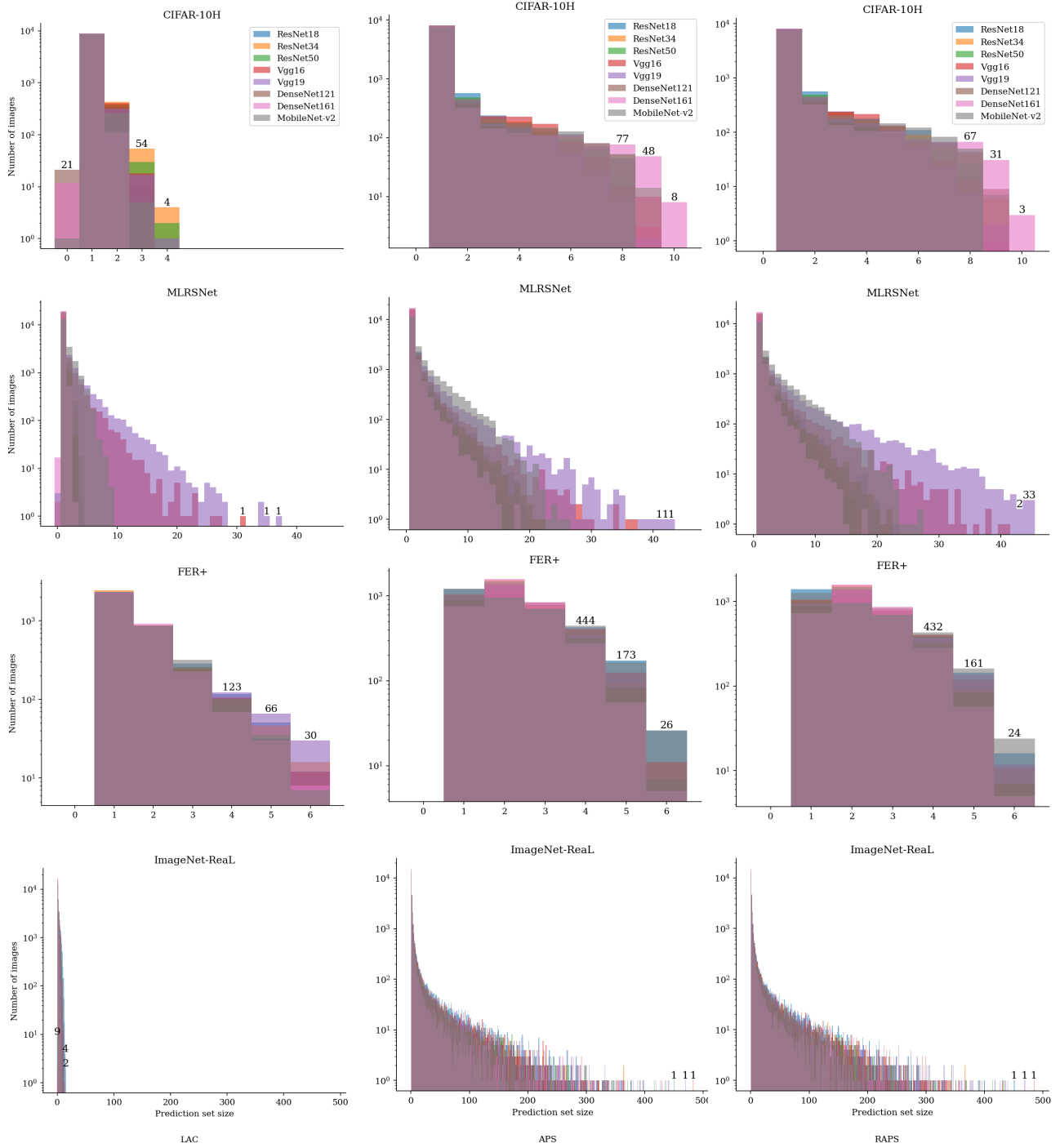


Figure A1. Distribution of prediction set sizes. The y-axis is log-scaled for easier visualization of the imbalanced counts. The count of the largest three prediction set sizes is shown on top of the bars. The three columns, from left to right, represent LAC, APS, and RAPS, respectively.

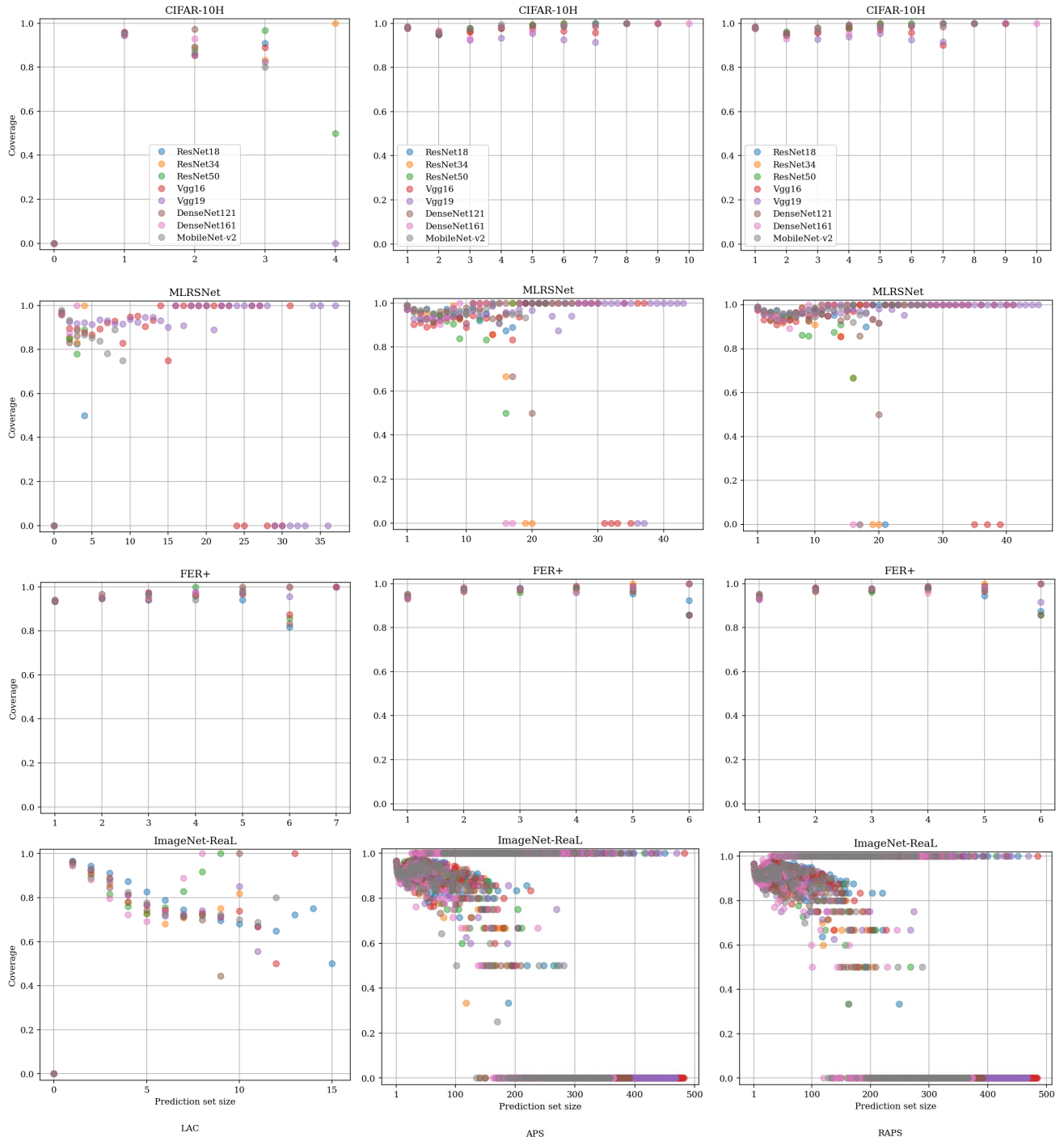


Figure A2. Coverage at different prediction set sizes. The X-axis shows prediction set sizes, and the Y-axis shows the coverage. The three columns, from left to right, represent LAC, APS, and RAPS, respectively.

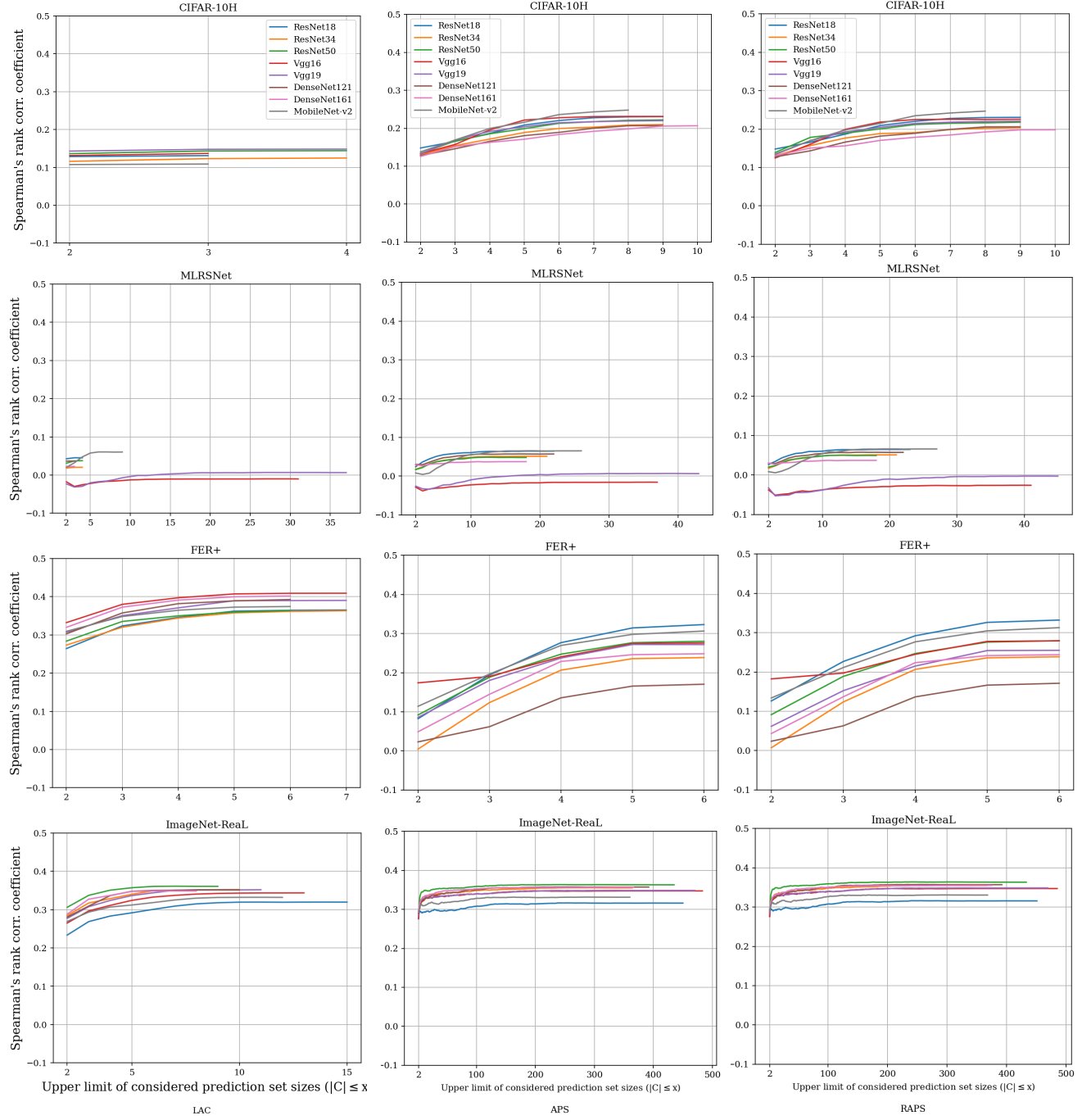


Figure A3. Spearman's rank correlation coefficient, r_s , $p < .001$, between prediction set sizes and class overlap with an increased prevalence of larger prediction sets. The X-axis shows the upper limit of the considered prediction set sizes ($|C| \leq x$), and the Y-axis shows Spearman's rank correlation coefficient. The three columns, from left to right, represent LAC, APS, and RAPS, respectively.

Table A1. Similarity between conformal predictors and human annotations on the CIFAR-10H dataset

| LAC | | | | APS | | | | RAPS | | | |
|-----------|--------|--------|-------------------------------|-----------|--------|--------|-------------------------------|-----------|--------|--------|-------------------------------|
| Precision | Recall | S. Acc | Hamming loss (\downarrow) | Precision | Recall | S. Acc | Hamming loss (\downarrow) | Precision | Recall | S. Acc | Hamming loss (\downarrow) |
| 0.967 | 0.661 | 0.099 | 0.426 | 0.935 | 0.705 | 0.107 | 0.419 | 0.935 | 0.705 | 0.107 | 0.419 |
| 0.966 | 0.667 | 0.099 | 0.429 | 0.936 | 0.707 | 0.109 | 0.415 | 0.941 | 0.702 | 0.107 | 0.418 |
| 0.971 | 0.667 | 0.098 | 0.431 | 0.945 | 0.704 | 0.105 | 0.423 | 0.950 | 0.699 | 0.103 | 0.426 |
| 0.972 | 0.667 | 0.098 | 0.429 | 0.943 | 0.707 | 0.105 | 0.422 | 0.948 | 0.703 | 0.103 | 0.424 |
| 0.973 | 0.665 | 0.098 | 0.430 | 0.955 | 0.694 | 0.101 | 0.429 | 0.954 | 0.695 | 0.101 | 0.428 |
| 0.974 | 0.656 | 0.099 | 0.428 | 0.951 | 0.697 | 0.105 | 0.425 | 0.952 | 0.696 | 0.104 | 0.425 |
| 0.974 | 0.658 | 0.099 | 0.428 | 0.943 | 0.703 | 0.111 | 0.421 | 0.949 | 0.697 | 0.107 | 0.422 |
| 0.975 | 0.664 | 0.098 | 0.431 | 0.939 | 0.709 | 0.107 | 0.421 | 0.939 | 0.709 | 0.107 | 0.422 |

Table A2. Similarity between conformal predictors and human annotations on the MLRSNET dataset

| LAC | | | | APS | | | | RAPS | | | |
|-----------|--------|--------|-------------------------------|-----------|--------|--------|-------------------------------|-----------|--------|--------|-------------------------------|
| Precision | Recall | S. Acc | Hamming loss (\downarrow) | Precision | Recall | S. Acc | Hamming loss (\downarrow) | Precision | Recall | S. Acc | Hamming loss (\downarrow) |
| 0.927 | 0.688 | 0.181 | 0.345 | 0.901 | 0.711 | 0.198 | 0.228 | 0.905 | 0.710 | 0.196 | 0.230 |
| 0.931 | 0.665 | 0.173 | 0.351 | 0.889 | 0.720 | 0.192 | 0.219 | 0.884 | 0.722 | 0.197 | 0.218 |
| 0.936 | 0.619 | 0.172 | 0.366 | 0.921 | 0.693 | 0.190 | 0.245 | 0.918 | 0.697 | 0.188 | 0.242 |
| 0.941 | 0.655 | 0.166 | 0.352 | 0.900 | 0.728 | 0.180 | 0.209 | 0.907 | 0.709 | 0.184 | 0.206 |
| 0.930 | 0.677 | 0.174 | 0.370 | 0.922 | 0.709 | 0.195 | 0.223 | 0.919 | 0.715 | 0.192 | 0.221 |
| 0.931 | 0.682 | 0.160 | 0.351 | 0.899 | 0.698 | 0.201 | 0.208 | 0.892 | 0.697 | 0.199 | 0.207 |
| 0.932 | 0.690 | 0.151 | 0.361 | 0.891 | 0.755 | 0.175 | 0.211 | 0.899 | 0.744 | 0.187 | 0.213 |
| 0.933 | 0.674 | 0.163 | 0.373 | 0.881 | 0.699 | 0.202 | 0.201 | 0.895 | 0.723 | 0.201 | 0.198 |

Table A3. Similarity between conformal predictors and human annotations on the FER+ dataset

| LAC | | | | APS | | | | RAPS | | | |
|-----------|--------|--------|-------------------------------|-----------|--------|--------|-------------------------------|-----------|--------|--------|-------------------------------|
| Precision | Recall | S. Acc | Hamming loss (\downarrow) | Precision | Recall | S. Acc | Hamming loss (\downarrow) | Precision | Recall | S. Acc | Hamming loss (\downarrow) |
| 0.918 | 0.710 | 0.146 | 0.364 | 0.753 | 0.775 | 0.196 | 0.234 | 0.785 | 0.766 | 0.185 | 0.267 |
| 0.934 | 0.698 | 0.144 | 0.365 | 0.756 | 0.762 | 0.186 | 0.214 | 0.754 | 0.763 | 0.187 | 0.213 |
| 0.933 | 0.707 | 0.141 | 0.376 | 0.758 | 0.776 | 0.182 | 0.239 | 0.760 | 0.776 | 0.181 | 0.241 |
| 0.934 | 0.717 | 0.137 | 0.384 | 0.756 | 0.795 | 0.186 | 0.249 | 0.761 | 0.794 | 0.185 | 0.253 |
| 0.928 | 0.713 | 0.144 | 0.374 | 0.760 | 0.782 | 0.186 | 0.238 | 0.740 | 0.788 | 0.192 | 0.224 |
| 0.928 | 0.712 | 0.139 | 0.377 | 0.740 | 0.784 | 0.190 | 0.217 | 0.739 | 0.784 | 0.191 | 0.217 |
| 0.936 | 0.713 | 0.136 | 0.386 | 0.727 | 0.785 | 0.190 | 0.209 | 0.723 | 0.786 | 0.192 | 0.205 |
| 0.918 | 0.716 | 0.143 | 0.375 | 0.758 | 0.782 | 0.194 | 0.242 | 0.765 | 0.781 | 0.191 | 0.252 |

Table A4. Similarity between conformal predictors and human annotations on the ImageNet-RealL dataset

| LAC | | | | APS | | | | RAPS | | | |
|-----------|--------|--------|-------------------------------|-----------|--------|--------|-------------------------------|-----------|--------|--------|-------------------------------|
| Precision | Recall | S. Acc | Hamming loss (\downarrow) | Precision | Recall | S. Acc | Hamming loss (\downarrow) | Precision | Recall | S. Acc | Hamming loss (\downarrow) |
| 0.571 | 0.892 | 0.002 | 0.370 | 0.568 | 0.934 | 0.012 | 0.417 | 0.567 | 0.934 | 0.012 | 0.416 |
| 0.670 | 0.885 | 0.001 | 0.481 | 0.631 | 0.930 | 0.008 | 0.480 | 0.629 | 0.931 | 0.008 | 0.478 |
| 0.736 | 0.882 | 0.001 | 0.559 | 0.678 | 0.931 | 0.007 | 0.529 | 0.679 | 0.931 | 0.007 | 0.529 |
| 0.628 | 0.887 | 0.002 | 0.434 | 0.604 | 0.933 | 0.010 | 0.453 | 0.603 | 0.934 | 0.010 | 0.452 |
| 0.643 | 0.886 | 0.002 | 0.452 | 0.611 | 0.934 | 0.010 | 0.462 | 0.612 | 0.934 | 0.010 | 0.462 |
| 0.684 | 0.884 | 0.001 | 0.494 | 0.632 | 0.934 | 0.008 | 0.479 | 0.632 | 0.934 | 0.008 | 0.479 |
| 0.763 | 0.876 | 0.001 | 0.593 | 0.705 | 0.921 | 0.005 | 0.552 | 0.702 | 0.923 | 0.005 | 0.548 |
| 0.625 | 0.887 | 0.002 | 0.430 | 0.604 | 0.930 | 0.008 | 0.452 | 0.599 | 0.932 | 0.009 | 0.447 |